Oral presentation | 3 Optics and Photonics：3.14 Optics and Photonics English Session

Fri. Mar 14, 2025 1:00 PM - 4:15 PM JST | Fri. Mar 14, 2025 4:00 AM - 7:15 AM UTC K508 (Lecture Hall Bldg.)

[14p-K508-1~12] 3.14 Optics and Photonics English Session

Nobuhiko Nishiyama(Science Tokyo), Haisong Jiang(Kyushu University)

1:00 PM - 1:15 PM JST | 4:00 AM - 4:15 AM UTC

[14p-K508-1]

Optical Performance Evaluation of Automotive AR Head-Up Displays

○(D)Manning Sun[1], Nathan Hagen[1], Yukitoshi Otani[1] (1.Utsunomiya Univ.)

English Presentation

1:15 PM - 1:30 PM JST | 4:15 AM - 4:30 AM UTC

[14p-K508-2]

Wavelet-LSTM Approach for Optical Surface Extension

○(D)Ke Chen[1], Hayasaki Yoshio[1] (1.Utsunomiya Univ. for Utsunomiya University)

English Presentation

1:30 PM - 1:45 PM JST | 4:30 AM - 4:45 AM UTC

[14p-K508-3]

Polarization-Sensitive Quantum Imaging Using an Entangled-Photon Source

○(D)Mousume Samad[1,2], Maki Shimizu[1], Yasuto Hijikata[1] (1.Saitama University, 2.Bangladesh Army University of Engineering and Technology (BAUET))

English Presentation

1:45 PM - 2:00 PM JST | 4:45 AM - 5:00 AM UTC

[14p-K508-4]

0^{th} and 1^{st} Mode Coupler Integrated Optical Mode Switch Using Nano-Pixel

○(D)Yuzhuang Xie[1], Weijie Li[1], Chengyou Cai[1], Haisong Jiang[1], Kiichi Hamamoto[1] (1.Kyushu Univ)

English Presentation

2:00 PM - 2:15 PM JST | 5:00 AM - 5:15 AM UTC

[14p-K508-5]

Terahertz guidance through 3D printed single bar nested hollow-core fiber

○(D)Muhammad Zain Siddiqui[1], Kohei Chiba[2], Yoshiaki Kanamori[2], Mustafa Ordu[1] (1.Bilkent Univ., 2.Tohoku Univ.)

English Presentation

2:15 PM - 2:30 PM JST | 5:15 AM - 5:30 AM UTC

[14p-K508-6]

Simultaneous Polarization and Wavelength Filtering in Negative Curvature Hollow Core Fibers

○Mustafa Ordu[1], Muhammad Zain Siddiqui[1], Ahmet Emin Akosman[2] (1.Bilkent Univ., 2.Roger Williams Univ.)

English Presentation

2:45 PM - 3:00 PM JST | 5:45 AM - 6:00 AM UTC

[14p-K508-7]

© 2025 JSAP

Sub-THz Signal Generation Device Based on Optical Difference Frequency Generation using $LiTaO_3$ Rectangular Waveguide

○(D)Ken Paramayudha[1], Reiji Hiraga[1], Yui Otagaki[1], Hiroshi Murata[1] (1.Mie Univ.)

Presentation by Applicant for JSAP Young Scientists Presentation Award English Presentation

3:00 PM - 3:15 PM JST | 6:00 AM - 6:15 AM UTC

[14p-K508-8]

Rational molecular design strategy to obtain locally excited and charge transfer characters aimed for dual enhancement of two-photon absorption cross-section and TADF activity

○(D)GomathiVinayakam Mageswari[1], Youhei Chitose[1], Ja-Hon Lin[2], Youichi Tsuchiya[1], Chihaya Adachi[1] (1.Kyushu Univ, 2.Nati Taipei Univ Tec)

English Presentation

3:15 PM - 3:30 PM JST | 6:15 AM - 6:30 AM UTC

[14p-K508-9]

Circularly polarized two-photon induced photoluminescence from single plasmonic nanoparticle

○Hyoyong Ahn[1], Khai Q. Le[1], Tetsuya Narushima[1], Junsuke Yamanishi[1], Ryeong Myeong Kim[2], Ki Tae Nam[2], Hiromi Okamoto[1] (1.Inst. for Molecular Science, 2.Seoul National Univ.)

English Presentation

3:30 PM - 3:45 PM JST | 6:30 AM - 6:45 AM UTC

[14p-K508-10]

Second harmonic generation of Bloch-type optical skyrmion

○(P)Sushanta Kumar Pal[1], A. Srinivasa Rao[1], Hiroko Yokota[2], Takashige Omatsu[1] (1.Chiba Univ., 2.Inst. of Science Tokyo)

Presentation by Applicant for JSAP Young Scientists Presentation Award English Presentation

3:45 PM - 4:00 PM JST | 6:45 AM - 7:00 AM UTC

[14p-K508-11]

Predicting Purcell Enhancement of quasi-Bound States in the Continuum with Spectral Parameters

○(P)JoshuaTinYau Tse[1], Taisuke Enomoto[1], Shunsuke Murai[1], Katsuhisa Tanaka[1] (1.Kyoto Univ.)

English Presentation

4:00 PM - 4:15 PM JST | 7:00 AM - 7:15 AM UTC

[14p-K508-12]

High-temperature spectroscopic infrared thermal emitters based on epitaxial cerium hexaboride thin films

○Andrea RuizPerona[1,2], Hiroyuki Yamada[1], Thien Duc Ngo[1], Tadaaki Nagao[1] (1.NIMS, 2.Hokkaido Univ.)

© 2025 JSAP

車載用 AR ヘッドアップディスプレイの光学性能評価

Optical Performance Evaluation of Automotive AR Head-Up Displays

○(D1)孫　漫凝[1]，ネイサン　ヘーガン[1]，大谷　幸利[1]

CORE, Utsunomiya Univ.[1]

○Manning Sun[1], Nathan Hagen[1], Yukitoshi Otani[1]

E-mail: dc247106@s.utsunomiya-u.ac.jp

We developed a compact optical setup for automotive AR-HUDs using a PMMA plano-concave mirror coated as a reflective surface. This design reduces system size while maintaining imaging quality. We evaluated the system's optical performance using the knife-edge method to measure the modulation transfer function (MTF), confirming its effectiveness for AR-HUD applications and its potential for further optimization.

1. はじめに

車載用拡張現実（AR）型ヘッドアップディスプレイは，ドライバーに情報を提供しつつも視界を遮ることなく安全な運転をサポートする技術である．この表示画像の品質は，情報の鮮明さと視認性に直接的な影響を与える．適切なコントラストの確保は，ドライバーが道路情報やナビゲーション情報を正確に理解するために不可欠である．コントラストの評価は，ディスプレイの性能を客観的に評価する上で重要となる．

本研究は，AR-HUD の Modulation Transfer Function (MTF) を求めるシステムの開発する．具体的には、車種ごとに異なるウインドガラスに対するためにフラットガラスと凹面反射ミラーを組み合わせることで AR 型ヘッドアップディスプレイの光学性能評価法を可能するシステムを構築する．

2. MTF 解析法と実験

ナイフエッジ MTF は，高コントラストなパターンの再現能力を評価する際に有用な手法である．ナイフエッジ MTF 計算は，まず白黒変換した ESF を求める．ESF（Edge Spread Function）は，エッジ像のピクセル値のプロファイルと考えて良い．傾いた ESF を微分して LSF（Line Spread Function）に変換後，LSF の合成を行う．図 1 は，PMMA ミラー導入前後の光学システムおよび成像結果の比較を示している．PMMA ミラーの導入により，光学システムのコンパクト化が可能になり，成像性能が向上していることが確認できる．

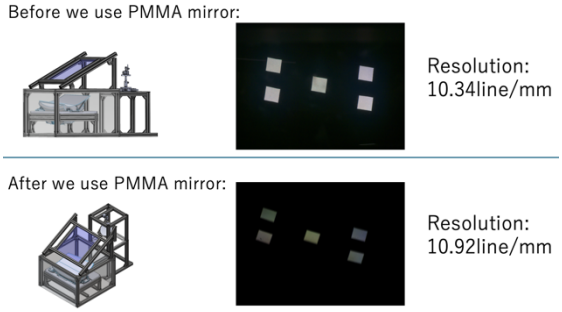

Fig 1 Comparison of the optical system and imaging results before and after introducing the PMMA mirror.

3. まとめ

PMMA 製平凹ミラーを用いた AR-HUD 評価システムを構築し，ナイフエッジMTF で性能を確認した．

参考文献

1）Nugent et al.: Optical Engineering, (2010).

© 2025年 応用物理学会

Wavelet-LSTM Approach for Optical Surface Extension

Utsunomiya Univ.[1] ○Chen Ke[1], Yoshio Hayasaki[1]

E-mail: chen_k@opt.utsunomiya-u.ac.jp

This study aims to address the edge effect problem commonly encountered in contact machining processes. By employing wavelet multiscale decomposition, the surface profile's frequency information is separated, and the separated frequency components are predicted using an LSTM neural network. The extended frequency components are then utilized to achieve surface profile extrapolation through reconstruction. Compared with traditional extrapolation methods, the proposed approach significantly improves the quality of the machined surface, offering a novel solution for high-precision machining.

1. Introduction

In ultra-large optical systems like astronomical telescopes (E-ELT, GMT) and space telescopes (JWST), components are too large to fabricate as a single piece. They are divided into subcomponents, machined separately, and assembled. This increases the total circumference, intensifying cumulative edge effects in contact machining, which significantly impacts precision..

2. Wavelet-LSTM Approach

The surface profile data of the component can be processed using wavelet multiscale analysis, decomposing the original row (or column) data into low-frequency components and high-frequency details at different scales. These components are treated as time series and modeled using deep learning methods to achieve component extension. After reconstructing the extended components, the original row (or column) data is correspondingly extended, fulfilling the goal of surface profile extrapolation.

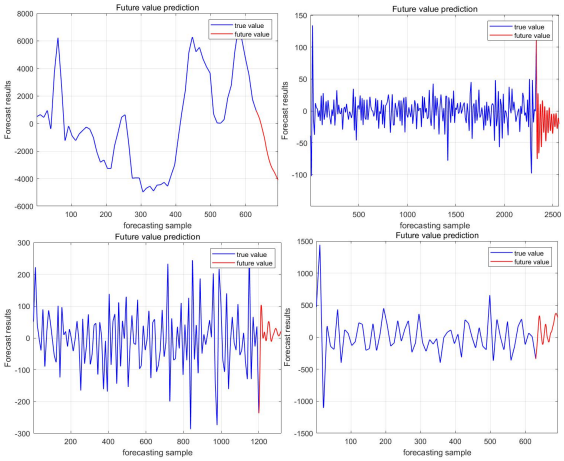

Fig 1 Take any row data of a surface shape, decompose it into four layers of components, and then use LSTM neural network to predict it, achieving the goal of extending the components.

Reference

1 ）Wang T, Huang L, Choi H, et al. RISE: robust iterative surface extension for sub-nanometer X-ray mirror fabrication[J]. Optics Express, 2021, 29(10): 15114-15132.

© 2025年 応用物理学会

Polarization-Sensitive Quantum Imaging Using an Entangled-Photon Source

Mousume Samad[1, 2], Maki Shimizu[1], Yasuto Hijikata[1]
[1]Graduate School of Science and Engineering, Saitama University.
[2] Department of Information and Communication Engineering, Bangladesh Army University of Engineering and Technology (BAUET)
E-mail: samad.m.128@ms.saitama-u.ac.jp; maki2@mail.saitama-u.ac.jp; yasuto@mail.saitama-u.ac.jp

Abstract: We experimentally demonstrate a quantum polarized microscopic technique utilizing a quantum-entangled photon source. Unlike classical methods, image contrast is constructed by coincident count of signal and idler photons. In the case that coincident count is recorded from both the signal and idler photons, the photon statistics is thermal state similarly as the case of black body radiation, but its peak intensity appearing in coincidentally counting is significantly high. While, when the coincident count is taken from either the signal or idler photon only, though the photon state exhibits thermal state again, the photon statistics becomes more dispersive and thereby its peak intensity is lowered. These different thermal states can be switched by perturbing the photon polarization, which enable us polarization-enhanced imaging. Since this approach achieves enhanced image contrast with minimal illumination power (on the order of Pico joule), offering a significant advancement in biomedical microscopy.

1. Experimental Set up and Methodology of Imaging: The schematic experimental setup of quantum polarized microscopy is illustrated in Fig. 1(a), utilizing a correlated photon pair source based on collinear type-II spontaneous parametric down-conversion (SPDC). Figure 1(b) schematically illustrates the coincidence count rates and the autocorrelation function $g^2(0)$ at zero delay of entangled photon pairs as a function of analyzer angle. Here, the value of $g^2(0)$ can be determined using the following equation [1]:

$$g^2(0) = \frac{R_{AB}(0)}{R_A \cdot R_B \cdot \Delta t} \quad (1)$$

where R_A, R_B, and R_{AB} are the count rate of the beam pass with the rotating analyser (channel A), the fixed analyser (channel B), and coincidence count rate of channel A and B, respectively and Δt is the coincident windows. We derive the values of $g^2(0)$ from the count rates, R_A, R_B, and R_{AB}. Since in the case that the coincidence rate is taken from both the signal and idler photons the time interval between pair of photons [Signal and Idler] is stretched compared to the Poisson case ($g^2(0)=1$) or super-Poisson ($g^2(0)>1$) [2], the photon-bunching is enhanced. Here, this photon state is called as 'hyper-Poisson state.' Whereas the super-Poisson state is prepared by blocking either the signal or the idler photon using an analyzer, which shows more dispersive photon statistics than hyper-Poisson state, resulting in a lower magnitude of bunching. The image contrast is constructed by modulating the polarizer angle, transitioning between hyper-Poisson and super-Poisson states. In general, the coincidence count rate follows a sinusoidal pattern with analyzer angle, and the sharp dip in $g^2(0)$ at coincidence rate minimum corresponds to a transition from hyper-Poisson to super-Poisson in photon states, producing image contrast. Since the sharpness of the dips in $g^2(0)$ correlates directly with image contrast, by setting the analyzer angle in sample port to be dip bottom, providing potentially superior sensitivity compared to conventional polarization-enhanced imaging methods.

2. Result and Discussion: To demonstrate our imaging method, a spiral retarder optical sample has been utilized. The two-dimensional (2D) images of the coincidence and autocorrelation are displayed in Fig 2 (a) and (b), respectively. As illustrated in the figures, coincidence image provides contrast across the entire sample; however, the contrast tends to decrease near the maximum and minimum value (represented by red and blue on the color scale bar, respectively). On the other hand, an autocorrelation image exhibits high contrast near the minimum value. However, due to the narrow range of analyzer angles that provides sufficient contrast, the area having near the maximum value, i.e. the region with low contrast is expanded. The signal-to-noise ratio (SNR) of this experiment was comparable to the SNR value reported in the similar work [3].

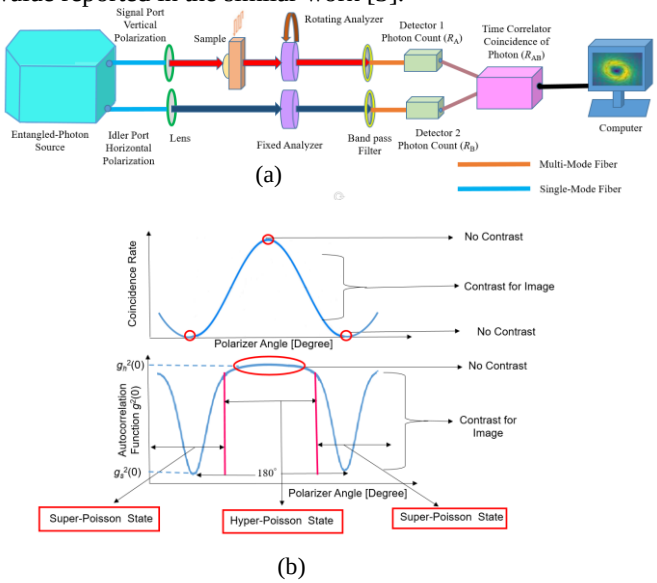

Fig. 1: Schematic illustrations of (**a**) Experimental set up (**b**) Coincidence rate and autocorrelation function at zero delay $g^2(0)$ as a function of polarization angle.

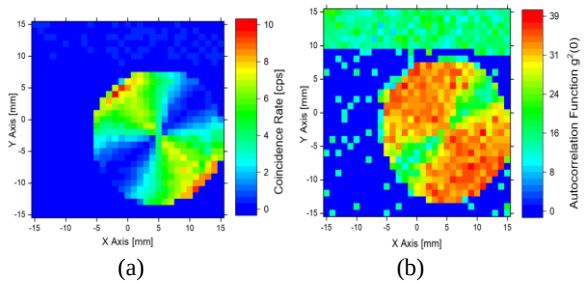

Fig. 2: (**a**) Coincidence image and **(b)** Autocorrelation image of the spiral retarder sample.

References:

[1] EDU-QOP1 (/M) Quantum Optics Kit. Available online: https://www.thorlabs.com (9th April, 2024).
[2] David, S.; Gregg J. Quantum Metrology, Imaging, and Communication. Springer: 2018. [https://doi.org/10.1007/978-3-319-46551-7].
[3] Defienne, H.; Ndagano, B.; Lyons, A.; Faccio, D. Polarization entanglement-enabled quantum holography. Nat. Phys., 2021, 17, 591-597.

© 2025年 応用物理学会

0th and 1st Mode Coupler Integrated Optical Mode Switch Using Nano-Pixel

Yuzhuang Xie, Weijie Li, Chengyou Cai, Haisong Jiang, and Kiichi Hamamoto
Interdisciplinary Graduate School of Engineering Sciences (I-EggS), Kyushu University
E-mail: xie.yuzhuang.573@s.kyushu-u.ac.jp

1. Introduction

An optical mode switch using nano-pixel for 0th and 1st modes has been investigated. One difficulty exits in the mode coupler as it must divide with securing phase difference in case of 1st order mode division, whereas couple them into proper 1st mode at the coupler [1-4]. As a result, proper mode-switching was confirmed even in case of utilizing nano-pixel mode coupler.

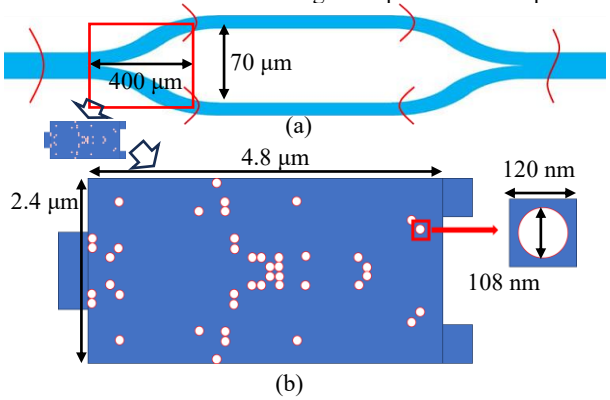

Fig. 1 Optical mode switch. (a) Conventional, and (b) proposed.

2. Concept of 0th and 1st mode coupler

So far, we have proposed and demonstrated optical mode switch of which the mode-splitter section was consisted of specially designed Y-branch. In our coupler design, the splitting must be carefully managed: the 0th mode is split into two 0th modes with a phase difference of 0, while the 1st mode is split into two 0th modes with a phase difference of π. The phase relationship must also be preserved when combining modes. This means maintaining the same phase or ensuring a phase difference of π based on the intended result. We optimized the coupler design for various lengths and selected the best-performing design.

3. Results and discussion

We designed nine different nano-pixel structures with dimensions of 2.4 × 1.2 μm^2, 2.4 × 2.4 μm^2 and 2.4 × 4.8 μm^2. For each structure, the split output port positions were set at distances of 0.3 μm, 0.6 μm and 0.95 μm from the center of the injection port. The pixel size is 120 nm each square and the air hole diameter is set to be 108 nm. The switch was built on silicon-on-insulator wafer and all simulations were carried using 2D-FDTD (finite-difference time-domain) method. In the design process, we employed a correlation coefficient method [5] to monitor the 0th mode splitting results and used symmetric structure to maintain required phase difference. Random pattern was used as the initial structure and direct-binary-search (DBS) method [6-8] was applied to optimize hole arrangement. All the optimized 1 × 2 nano-pixel field coupler demonstrated low excess loss (less than 1 dB) while maintaining 0th mode output. We replaced the traditional Y-branch structures with nano-pixel structures in optical mode switch and selected the best-performing structure which has a low excess loss and performs well in maintaining the output 0th mode and 1st mode. The optimized was determined to be 2.4 × 4.8 μm^2 with output ports positioned 0.95μm from centre. Figure 2 shows 0th mode situation. The output power is 91.803 % and excess loss is 0.371 dB. The output mode successfully maintains 0th mode.

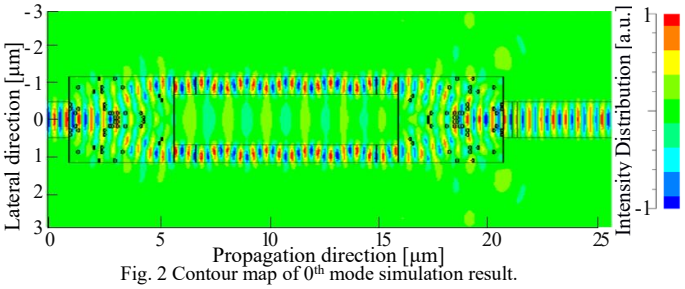

Fig. 2 Contour map of 0th mode simulation result.

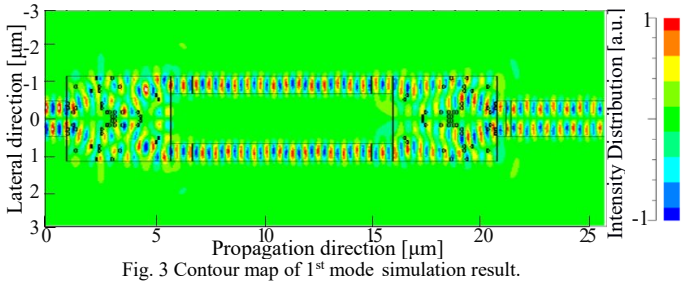

Fig. 3 Contour map of 1st mode simulation result.

Figure 3 illustrates 1st mode situation, where the output power is 95.675 % and excess loss is 0.192 dB. The output mode successfully maintains 1st mode. The primary source of excess loss was identified as scattering light. By comparing the nine patterns, we conclude that for optical multi-mode switch, a relatively long structure effectively balances the splitting results for different modes. Furthermore, due to varying power distribution of different mode, a relatively far apart of output ports perform better.

4. Conclusion

To design a compact optical mode switch capable of simultaneously handling the 0th and 1st modes, we proposed using nano-pixel structure. Compared to conventional 400 × 70 μm^2 Y-branch, it has compact size of 2.4 × 4.8 μm^2. Simulation results show that in 0th mode situation, the excess loss is 0.371 dB and output maintain 0th mode. In the 1st mode situation, the excess loss is 0.192 dB and output maintain 1st mode.

Acknowledgment

A part of this was supported by Kakenhi #24K07608.

References

[1] R. Imansyah, et. al., JJAP., **55**, 08RB06, 2016
[2] K. Hamamoto, et. al., APC/PS, PTh1D.4, 2017
[3] H. Ma, et. al., Opt. Expr, **28**, 17010, 2020
[4] H. Jiang, et. al.,” IEICE Trans. Electron., **E100-C**, 782, 2017
[5] Y. Xie, et. al., Tech. Dig. MOC, PO-62, 2023
[6] H. Jia, et. al., Tech. Dig. CLEO, STu4D.3, 2021
[7] T. Fujisawa, et. al., OSA Contin, **4**, 1258, 2021
[8] K. Kojima, et. al., IPR2017, ITu1A.4, 2017

© 2025年 応用物理学会

Terahertz guidance through 3D printed single bar nested hollow-core fiber

○Muhammad Zain Siddiqui[1], Kohei Chiba[2], Yoshiaki Kanamori[2], and Mustafa Ordu[1]
[1] UNAM - Institute of Materials Science and Nanotechnology, Bilkent University, Ankara, Türkiye
[2] Department of Robotics, School of Engineering, Tohoku University, Sendai, Japan
E-mail: ordu@unam.bilkent.edu.tr and ykanamori@tohoku.ac.jp

1. Introduction

Terahertz (THz) waves spanning from *0.1* to *10 THz* frequencies possess excellent properties, which makes them suitable for potential applications, including spectroscopy, data transmission, imaging, and security monitoring [1], [2], [3]. The THz spectrum is susceptible to high material absorption losses for numerous materials; therefore, propagation in hollow-core fibers (HCFs) has attracted much attention. Fabrication of THz waveguides through 3D printing provides a straightforward and cost-effective method for developing precise and intricate HCF designs. In this study, a single bar-nested tubular fiber (BNTF) is numerically designed and fabricated using fused deposition modeling (FDM) for short-range THz wave guidance. The four-tube cyclic olefin copolymer (TOPAS) based fiber showed good transmission characteristics in between *0.65* to *0.8 THz* range.

2. Fiber Design and Simulation Method

The BNTF design is illustrated in Fig. 1(a) with design parameters including core diameter, *D*, cladding tube diameter, *d*, bar distance, *s*, and strut thickness, *t*. COMSOL Multiphysics software with an electromagnetic wave frequency domain (EWFD) module was utilized for numerical analysis. For precise and accurate results, mesh size and perfectly matched layer (PML) were optimized through convergent studies at *0.75 THz*.

3. Results and Discussion

Through parametric studies, the BNTF design was optimized at $D = 3$ *mm*, $d = 4.2$ *mm*, $s/d = 0.4$, and $t = 0.29$ *mm*. Fig. 1(c) compares the calculated TL (total loss), a sum of CL (confinement loss), and EML (effective material loss) with the bulk material loss of TOPAS [4]. The designed TL of BNTF is about two orders of magnitude lower than the bulk material loss. The optimized design parameters of BNTF were used to 3D print the THz fibers through FDM. The cross-sectional image of 3D printed BNTF is shown in Fig. 1(b). BNTF fibers in lengths of *70 mm, 101 mm, 122 mm,* and *169 mm* were fabricated. These fibers were characterized through THz frequency-domain spectroscopy. The transmission measurements of all the fibers are depicted in Fig. 1(d). The fibers exhibit satisfactory THz wave guidance, measuring losses between *5.7* to *11.6 dB/m* with an average loss of *8.6 dB/m* between *0.65* and *0.8 THz*. The measured average loss is higher than the calculated TL due to fabrication-related issues but remains substantially lower than the TOPAS bulk material loss.

Acknowledgment

Authors acknowledge the assistance of Taiyu Okatani (Tohoku University) for initial THz optical characterization. This work is supported by JSPS Bilateral Program Number JPJSBP120239401 and TUBITAK Project Number 222N072.

References

[1] M. A. Mollah, *et al.*, "Novel hollow-core asymmetric conjoined-tube anti-resonant fiber for low-loss THz wave guidance," *OSA Contin.*, vol. 3, no. 5, pp. 1169–1176, May 2020.
[2] W. Talataisong *et al.*, "Hollow-core antiresonant terahertz fiber-based TOPAS extruded from a 3D printer using a metal 3D printed nozzle," *Photonics Res.*, vol. 9, no. 8, pp. 1513–1521, Aug. 2021.
[3] A. Khan, *et al.*, "Elliptical cladding elements in negative curvature hollow-core fiber for low-loss terahertz guidance," in *2022 International Conference on Information Science and Communications Technologies (ICISCT)*, Sep. 2022.
[4] K. Nielsen, *et al.*, "Bendable, low-loss Topas fibers for the terahertz frequency range," *Opt. Express*, vol. 17, no. 10, pp. 8592–8601, May 2009.

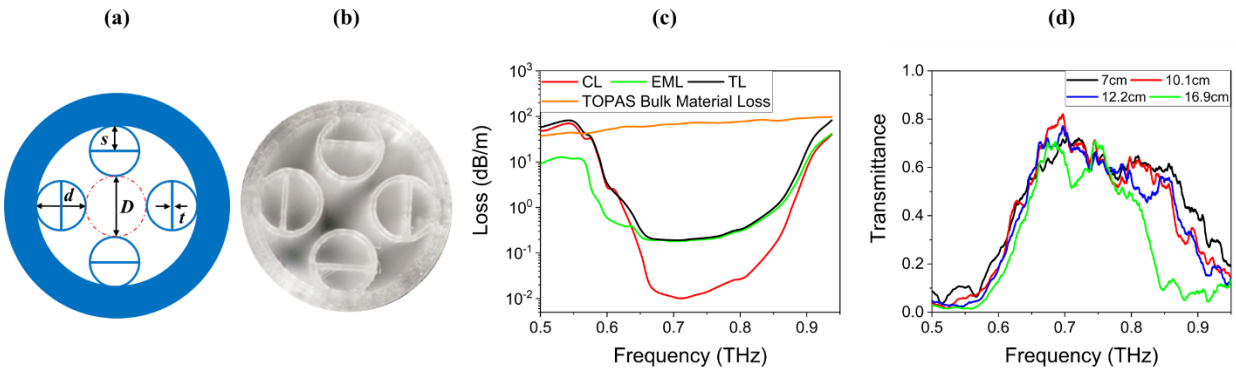

Figure 1 (a) A schematic of BNTF with design parameters. (b) A cross-sectional image of 3D printed BNTF. (c) TOPAS bulk material loss comparison with simulated losses, which includes confinement loss (CL), effective material loss (EML), and total loss (TL) in the range of 0.5 to 0.95 THz. (d) Transmittance curve of fabricated fiber for four different fiber lengths in the range of 0.5 to 0.95 THz.

© 2025年 応用物理学会

Simultaneous Polarization and Wavelength Filtering in Negative Curvature Hollow Core Fibers

○Mustafa Ordu[1,*] and Muhammad Zain Siddiqui[1], Ahmet Emin Akosman[2]
[1] UNAM - Institute of Materials Science and Nanotechnology, Bilkent University, Cankaya, Ankara 06800, Türkiye
[2] School of Engineering, Computing and Construction Management, Roger Williams University, Bristol, RI 02809, USA
E-mail: *ordu@unam.bilkent.edu.tr

1. Introduction

Negative curvature hollow-core fibers (NCFs) have promising applications spanning UV to THz regimes due to their superior properties, such as ultra-low loss transmission, low non-linearity, high data transfer rate, and high power laser delivery [1]. Polarization-maintaining (PM) property is extensively explored in NCFs by employing asymmetry fiber core for the near-IR region [2], [3]. However, frequency-selective transmission remains to be investigated in NCFs like in solid core fibers [4], [5]. This study introduces a novel design of pole-supported nested tubular polarization-maintaining NCF (P-PMNCF), capable of simultaneous PM operation and wavelength filtering in the near-IR region. The six-tube silica fiber (P-PMNCF) exhibits an asymmetric core due to nest elements with and without pole anchors in the vertical and horizontal directions, respectively, enabling simultaneous PM and spectral filtering operations. The frequency selectivity is encountered only for the vertical polarization due to light coupling to the pole anchors [6].

2. Fiber Design and Simulation Method

The cross-sectional image of the proposed P-PMNCF is shown in Fig. 1(a). The fiber design parameters include core size, D_x, and D_y, cladding tube diameter, d_1, nested tube diameter, d_2, pole length, L_p, strut thickness, t_1, and outer cladding tubes thickness in horizontal direction, t_2. The core size D_x is numerically optimized at a $\lambda = 1.55\ \mu m$ targeting the filtered wavelength losses below $0.1\ dB/km$ and birefringence $\geq 10^{-5}$. The numerical simulations were performed using the finite element-based electromagnetic wave frequency domain (EWFD) module in COMSOL Multiphysics. The mesh sizes and perfectly matched layers (PMLs) were optimized according to ref. [6].

3. Results and Discussion

Confinement losses and birefringence are affected inversely by changes in core size [2]. a trade-off must be considered between acceptable losses and desired birefringence. Using previously optimized fiber parameters, $d_1 = 25\ \mu m$, $d_2 = 18\ \mu m$, $t_1 = 0.40\ \mu m$, $t_2 = 0.62\ \mu m$, and $L_p = 5.7\ \mu m$, the core diameter was initially investigated by keeping D_x and D_y equal. It was found that the core diameter did not produce the desired filtered wavelength losses and birefringence, simultaneously. Therefore, core ellipticity was introduced for D_x while keeping D_y constant at $30\ \mu m$. Fig. 1(b) and 1(c) show a tradeoff is reached at $D_x = 27.75\ \mu m$. Filtered wavelength losses below $0.1\ dB/km$ and birefringence $\geq 10^{-5}$ are achieved in the final optimized design. The optimized fiber shows two orders of magnitude improvement in birefringence.

References

[1] C. Wei, *et al.*, "Negative curvature fibers," *Adv. Opt. Photonics*, vol. 9, no. 3, pp. 504–561, Sep. 2017.
[2] S. A. Mousavi, *et al.*, "Broadband high birefringence and polarizing hollow core antiresonant fibers," *Opt. Express*, vol. 24, no. 20, pp. 22943–22958, Oct. 2016.
[3] Y. Hong *et al.*, "Birefringent, low loss, and broadband semi-tube anti-resonant hollow-core fiber," *Opt. Lett.*, vol. 48, no. 1, pp. 163–166, Jan. 2023.
[4] S. Aleshkina *et al.*, "Spectral filtering in single-mode fibers using resonant coupling with absorbing rods," *Opt. Lett.*, vol. 46, no. 6, pp. 1458–1461, Mar. 2021.
[5] J. Gamble, *et al.*, "Frequency selective low-loss transmission in negative curvature hollow-core fibers," *Phys. Scr.*, vol. 99, no. 5, p. 055535, Apr. 2024.
[6] M. Z. Siddiqui, *et al.*, "Enhancing polarization maintenance and spectral filtering in negative curvature hollow-core fibers," *Photonics Nanostructures - Fundam. Appl.*, vol. 58, p. 101221, Feb. 2024.

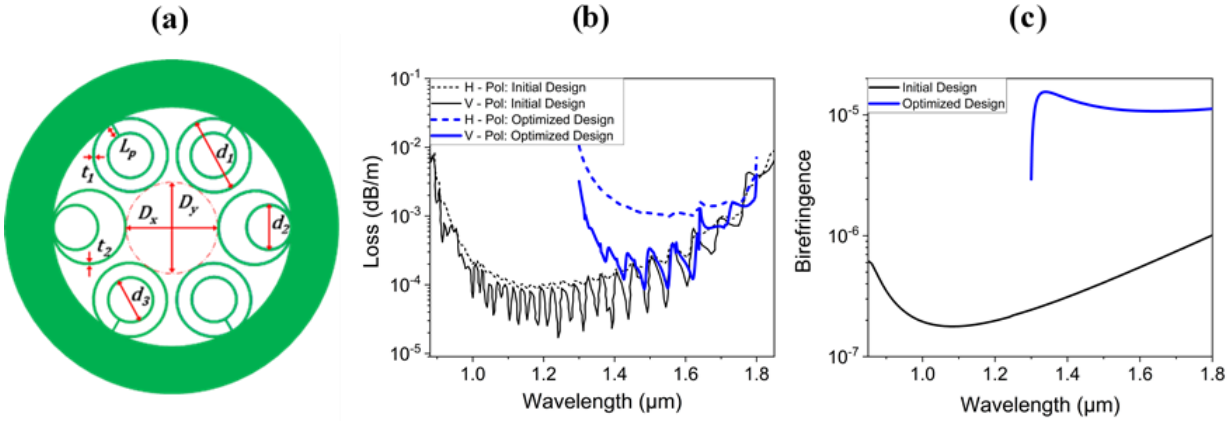

Figure 1 (a) A cross-sectional image of P-PMNCF with design parameters. (b) Confinement losses comparison between initial design and optimized design. (c) Birefringence comparison between initial design and optimized design. Optimized design refers to results at $D_x = 27.75\ \mu m$

© 2025年 応用物理学会

Sub-THz Signal Generation Device Based on Optical Difference Frequency Generation using $LiTaO_3$ Rectangular Waveguide

Mie Univ. , ◦Ken Paramayudha, Reiji Hiraga, Yui Otagaki, Hiroshi Murata

E-mail: 422de01@m.mie-u.ac.jp

The sub-THz spectrum offers significant potential for advanced applications, such as remote sensing and high-speed wireless communication, creating a need for efficient signal generation methods. In this study, we report on a sub-THz signal generation device that utilizes difference frequency generation (DFG) through nonlinear optical effects, combined with a rectangular waveguide structure. The device is based on a polarization-reversed $LiTaO_3$ crystal and optical waveguides enclosed in metal walls, allowing customized spatial distribution and phase relationship of the induced nonlinear polarization within the crystal. This design enables the selective coupling of optical DFG signals into sub-THz waveguide modes.

The basic structure of the device is shown in Fig. 1. A $LiTaO_3$ with a width (*a*) of 0.4 mm, a height (*b*) of 0.3 mm, a length of 20 mm and a polarization reversal period of 1.1 mm is designed to generate 100 GHz signal. Due to the second-order nonlinear optical effect, a nonlinear polarization is induced in the crystal, oscillating at the difference frequency of two light waves propagating inside the optical waveguide, thereby generating a sub-THz wave. This generated wave is coupled with the TE_{10} mode of the rectangular waveguide and can be extracted as the output of the waveguide circuit. The output can be coupled from the end of the waveguide using a horn antenna or by attaching sub-THz devices, such as a waveguide coupler [1] or an antenna, directly to the DFG device.

The expected DFG frequency response of the device is depicted in Fig. 2, which combines contributions from the cavity resonance of the rectangular waveguide and the quasi-phase matching bandwidth. A preliminary experiment to evaluate the resonance characteristics of the DFG waveguide has been conducted, as shown in Fig. 3. This result confirms a cavity resonance at 100 GHz. The measurement results of DFG signal generation will be presented during the presentation.

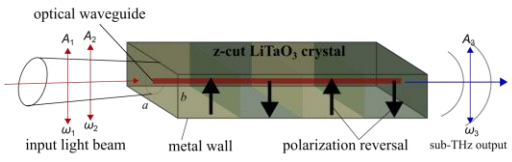

Fig. 1 Basic device structure

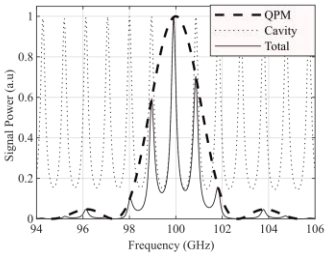

Fig. 2 DFG frequency response

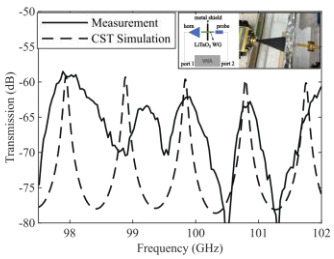

Fig. 3 Resonance characteristics

Acknowledgement
This work was supported in part by the research and development project entitled with ‘THz and optical wireless aggregation research & development for B5G (Toward-B5G)’ from NICT, Japan.

Reference

[1] K. Paramayudha et al, “Design of sub-THz signal generation device based on optical difference frequency generation using T-branch $LiTaO_3$ and Al_2O_3 rectangular waveguide”, *Proc. PEM 2023*, PEM2023-M3, pp 11-14, Nov. 2023, Sapporo, Japan.

© 2025年 応用物理学会

Rational molecular design strategy to obtain locally excited and charge transfer characters aimed for dual enhancement of two-photon absorption cross-section and TADF activity

Gomathi Vinayakam Mageswari[1], Youhei Chitose[1], Ja-Hon Lin[2], Youichi Tsuchiya[1], and Chihaya Adachi[1]

[1]*Center for Organic Photonics and Electronics Research (OPERA), Kyushu University, 744 Motooka, Nishi-Ku, Fukuoka 819-0395, Japan*

[2]*Department of Electro-Optical Engineering, Advanced Nanophotonics Technology Laboratory, National Taipei University of Technology, Taipei 10608, Taiwan*

E-mail: mageswari@opera.kyushu-u.ac.jp

The pursuit of an effective molecular design for highly efficient thermally activated delayed fluorescence (TADF) emitters with two-photon absorption (2PA) character is hampered by the concurrent achievement of a small singlet-triplet energy gap (ΔE_{ST}) and a large oscillator strength (f) with hybridized LE and CT characters.[1] Here, by introducing a terephthalonitrile unit into a sterically crowded D-π-D structure, we designed TADF emitters with 2PA phenomenon by bearing hybrid electronic excitation character (**Fig. 1**). This rational molecular design was achieved through a main π-conjugated donor-acceptor-donor (π-DAD) in line with locally excited features and an auxiliary N-donor-acceptor-donor (N-DAD) with charge transfer (CT) character, highly balancing the TADF phenomenon by a small ΔE_{ST} and maintaining high 2PA cross-section with a large f value. [2] Moreover, the incorporation of naphthyl groups was found to manipulate the emission properties without surrendering the Φ_{PL} values. A near-unity Φ_{PL} value with a large radiative decay rate over an order of magnitude higher than the intersystem crossing (ISC) rate and a high horizontal orientation ratio ($\Theta_{//}$) of 0.95 were simultaneously obtained for the emitter of **TPCz2NP**. By overcoming the trade-off of molecular design between TADF and 2PA materials with a rigid molecular framework, an optimal goal of efficient OLED and moderate 2PA ability was successfully achieved. The organic light-emitting diode (OLED) fabricated with this material exhibits a record-high maximum external quantum efficiency (EQE) of 25.4%. Further, we confirmed that the hybridized molecule with balanced LE and CT characters also gave rise to an enhancement of the 2PA cross-section (σ^2) value up to 143 GM at 850 nm, which is the highest value among the reported TPN-based TADF emitters with EQE_{max} values exceeding 25%. [3] These findings offer a venue for designing high-performance TADF emitters with exceptional 2PA properties, expanding future OLED material design.

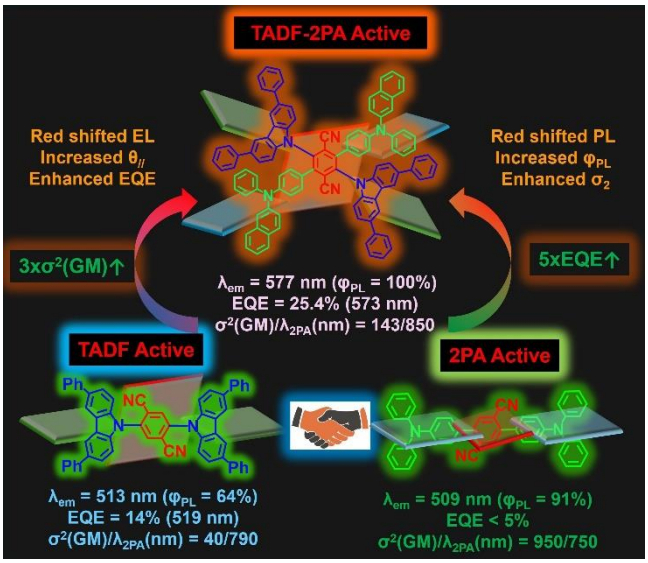

Fig. 1: Schematic representation of molecular design

References

(1) H. Uoyama et al. *Nature*, **2012**, 492, 234−238.
(2) C.-H. Chen et al. *Dyes and Pigments*, **2020**, 175, 108143.
(3) J. Zhang et al. *ACS Appl. Mater. Interfaces*, **2016**, 8, 11355-11365.

© 2025年 応用物理学会

Circularly polarized two-photon induced photoluminescence from single plasmonic nanoparticle

Institute for Molecular Science[1], Seoul National University[2], ◦Hyo-Yong Ahn[1], Khai Q. Le[1], Tetsuya Narushima[1], Junsuke Yamanishi[1], Ryeong Myeong Kim[2], Ki Tae Nam[2], and Hiromi Okamoto[1]

E-mail: hyahn@ims.ac.jp

Materials generating circularly polarized luminescence (CPL) have been studied mostly in the category of organic dye molecules and their assemblies, or organic-inorganic hybrid systems. In these cases, the chirality of the overall luminescent system arises from the molecular chirality, for example, by using organic dyes with inherent chirality or by incorporating chiral ligands or assemblies. Recently, it has been proposed that the localized chiral electromagnetic fields of plasmonic nanostructures and metamaterials can transfer the chirality to organic dyes or quantum dots, which can be utilized for CPL generation. In the present study, we demonstrate a novel approach for "all-in-one" CPL-generating materials using chiral plasmonic nanostructures[1]. Despite being composed of a single element, the chiral Au nanoparticles are capable of simultaneously providing the photoluminescence process attributed to the electronic band structure of Au, the optical enhancement in the near-field regime based on the localized surface plasmon resonance, and the chiro-optical response arising from the nanoscale chiral structure. We found that chiral Au helicoid nanoparticles exhibit circularly polarized two-photon induced photoluminescence (TPI-PL, Fig. 1), with a very high luminescence dissymmetry factor (*g*-factor) of ~0.7, as single-component nanoparticles. Using electromagnetic simulations, we confirmed that the characteristic chiral gap structure of the helicoid nanoparticle is the local emission site contributing to the highly chiral light emission. The experimentally observed emission intensity and *g*-factor spectra were consistent with those expected from the simulation model. We believe that this work provides a new route to novel CPL-generating materials with strong dissymmetry and holds promise for various applications such as bioimaging, sensing, anti-counterfeiting, and display technologies.

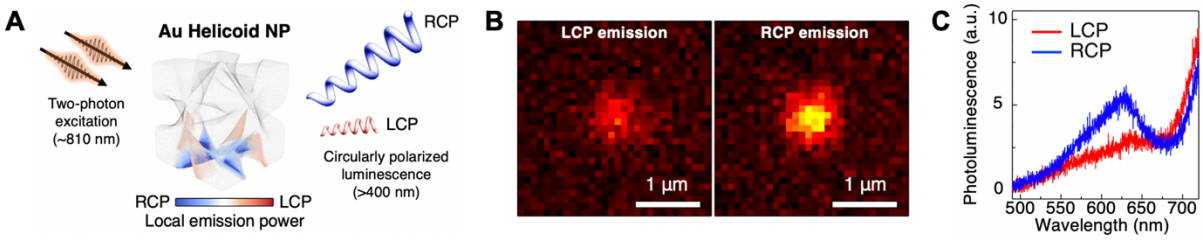

Fig. 1 (A) Schematic illustration of chiral light emission by TPI-PL process of Au helicoid NP. **(B)** TPI-PL images for left and right circularly polarized emission of a single Au helicoid NP. **(C)** TPI-PL spectra of the Au helicoid NP.

[1] Hyo-Yong Ahn, et al., *Adv. Opt. Mater.* **12**, 2400699 (2024)

© 2025年 応用物理学会

Second harmonic generation of Bloch-type optical skyrmion

Sushanta Kumar Pal[a,b], A. Srinivasa Rao[a,b], Hiroko Yokota[c], Takashige Omatsu[a,b,*]

[a]Graduate School of Engineering, Chiba University, Chiba 263-8522, Japan

[b]Molecular Chirality Research Center, Chiba University, Chiba 263-8522, Japan

[c]Institute of Science Tokyo, Kanagawa 152-8552, Japan

E-mail: omatsu@faculty.chiba-u.jp

Optical skyrmions, which possess all possible polarization states mapped on a three-dimensional Poincaré sphere in a two-dimensional physical space, have been studied as emerging structured light fields. The optical skyrmions are promising to develop new fundamentals and advanced applications, such as exotic light-matter interactions [1, 2], high-resolution imaging [3], and information processing [4].

In this presentation, we demonstrate, for the first time to the best of our knowledge, the second harmonic generation of Bloch-type optical skyrmion. A picosecond laser (wavelength: 1064 nm, pulse width: 10 ps, pulse repetition frequency: 1 MHz) was used and its output was converted into a Bloch-type optical skyrmion by employing a Mach-Zehnder-type polarization interferometer. The generated optical skyrmion exhibited a top-hat-shaped spatial intensity profile and a skyrmion number of 0.79. The optical skyrmion was then focused onto a nonlinear β-BaB_2O_4 crystal with a thickness of 1 mm. As shown in Fig. 1, the second-harmonics showed an elliptical spot with minor and major axes about 1/6 and 1/3 of the fundamental spot diameter, indicating its super-resolution property. This super-resolution property of the frequency-doubled optical skyrmion will provide the potential to develop a high spatial resolution second harmonics microscope.

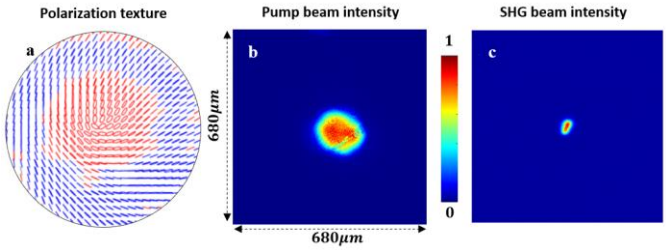

Fig. 1: (a) Spatial polarization texture and (b) normalized intensity profile of 1.06 μm Bloch-type optical skyrmion. (c) Spatial intensity profile of the frequency-doubled optical skyrmion.

[1] R. Tamura, P. Kumar, A. S. Rao, K. Tsuda, F. Getzlaff, K. Miyamoto, N. M. Litchinitser, T. Omatsu, "Direct imprint of optical skyrmions in azopolymers as photoinduced relief structures," APL Photonics **9**, 04604 (2024).

[2] R. Tamura, A. S. Rao, N. M. Litchinitser, T. Omatsu, "Three-dimensional projection of optical Hopfion textures in a material," ACS Photonics **11**(11), 4958-4965 (2024).

[3] L. Du, A. Yang, A. V. Zayats, X. Yuan, "Deep-subwavelength features of photonic skyrmions in a confined electromagnetic field with orbital angular momentum," Nat. Phys. **15**, 650-654 (2019).

[4] Z. Wan, H. Wang, Q. Liu, X. Fu, Y. Shen, "Ultra-Degree of freedom structured light for ultracapacity information carriers," ACS Photonics **10** (7), 2149-2164 (2023).

© 2025年 応用物理学会

Predicting Purcell Enhancement of quasi-Bound States in the Continuum with Spectral Parameters

Kyoto Univ. [1], ◦Joshua T. Y. Tse[1], Taisuke Enomoto[1], Shunsuke Murai[1], Katsuhisa Tanaka[1]

E-mail: tse@dipole7.kuic.kyoto-u.ac.jp

1. Introduction

The Purcell effect describes the enhancement of spontaneous emission of quantum emitters inside an optical cavity.[1] Optical cavities function to both increase the local density of states (LDOS) for enhanced spontaneous emission rate and redirect the emitted photons to specific out-coupling channels.[2,3] The Purcell enhancement is proportional to Q/V, i.e. the quality factor Q divided by the effective modal volume V, which represents the temporal and spatial confinement of the optical cavity respectively. While Q is straightforward to measure, V was known to be difficult to determine experimentally or analytically.

Bound states in the continuum (BIC) are optical resonances that are energetically compatible with free space but de-coupled from free space due to symmetry mismatch. The structures that support BIC can be detuned slightly to break the symmetry mismatch and create quasi-BIC that exhibit extraordinarily high Q. In this work, we analyzed the Purcell effect from quasi-BIC utilizing our analytical model that predicts the photoluminescence enhancement (PLE) with spectral parameters. We also explored the dependency of the PLE on different resonance characteristics of the quasi-BIC that significantly modulates the effectiveness of the quasi-BIC for enhancing luminescent processes.

2. Analytical Modelling of Purcell Enhancement

We recently reported about our new analytical model that predicted the averaged Purcell enhancement factor of the optical cavity with parameters fitted from spectral measurements.[4] In particular, the PLE was given by:

$$PLE(\omega_0) = \frac{c\Gamma_{rad}}{\omega_0 t {\Gamma_{tot}}^2}\frac{\Gamma_{abs,dye}}{\kappa}$$

where ω_0 is the resonant frequency, t is the dye layer thickness, κ is the extinction coefficient of the dye layer, and c is the speed of light in vacuum. $\Gamma_{tot} = \Gamma_{rad} + \Gamma_{abs,dye} + \Gamma_{abs,NP}$ is the total decay rate where Γ_{rad} is the radiative decay rate, $\Gamma_{abs,dye}$ and $\Gamma_{abs,NP}$ are the absorptive decay rates contributed by the dye layer and the nanoparticles. This model was subsequently verified by numerical simulations and photoluminescence measurement results.

3. Purcell Enhancement of quasi-BIC

We apply our analytical model to analyze the Purcell effect and the out-coupling of the enhanced luminescence. We simulated the quasi-BIC modes on bipartite silicon nanoparticle arrays with the finite-difference time-domain (FDTD) method. As shown in Fig. 1, the PLE first increased sharply as the detuning d was introduced, but as d further increases, the PLE reached a maximum and decreases for larger d. The initial increase was due to the increase in out-coupling efficiency while the decrease in Q reduced the PLE for larger d.

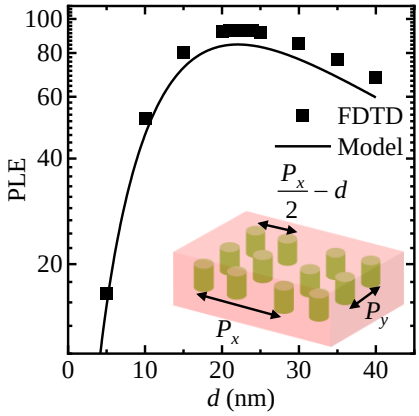

Figure 1. The FDTD simulated PLE and the PLE predicted by the analytical model was plotted against the detuning d. The inset illustrates the bipartite nanoparticle array that supports the quasi-BIC mode.

We also analyzed the quasi-BIC modes supported on asymmetric metasurfaces fabricated with glancing angle deposition. Due to the asymmetric shape of the nanoparticles in the metasurface, asymmetry was induced in Γ_{rad} about x-axis, and the BIC condition was also shifted from normal incident to 0.9°.

4. Conclusions

In conclusion, we developed an analytical model that describes the Purcell effect on quasi-BIC cavities and predicted the PLE that can be observed from the quasi-BIC modes. The spectral parameters were also analyzed to reveal the influence of Γ_{rad} on the PLE. This result presents a useful analytical framework for optimizing quasi-BICs for luminescence applications.

References

[1] E. M. Purcell, Phys. Rev. **69**, 681 (1946).
[2] C. Sauvan, J. P. Hugonin, I. S. Maksymov, and P. Lalanne, Phys. Rev. Lett. **110**, 237401 (2013).
[3] M. Ramezani, G. Lozano, M. A. Verschuuren, and J. Gómez-Rivas, Phys. Rev. B **94**, 125406 (2016).
[4] J. T. Y. Tse, S. Murai, and K. Tanaka, *Interpreting Purcell enhancement of non-Hermitian metasurfaces with spectral parameters*, Phys. Rev. A, accepted (2024).

© 2025年 応用物理学会

High-temperature spectroscopic infrared thermal emitters based on epitaxial cerium hexaboride thin films

National Institute of Material Science (NIMS) [1], Hokkaido University[2],

○Andrea Ruiz-Perona[1, 2], Hiroyuki Yamada[1], Thien Duc Ngo[1], Tadaaki Nagao[1, 2]

E-mail: NAGAO.Tadaaki@nims.go.jp

This research explores the development of plasmonic perfect absorbers capable of selectively emitting infrared radiation with narrow spectral resolution, essential for applications like plasmon-enhanced vibrational spectroscopy, thermophotovoltaics, and gas sensor light sources. While metallic refractory materials offer outstanding chemical and structural stability at high temperatures, their optical properties are inferior to those of plasmonic metals such as Au, Cu, and Al. These metals, despite their superior optical performance, have lower melting points and are prone to oxidation, limiting their effectiveness in high-temperature thermophotonics applications. To address the need for materials exhibiting strong plasmonic responses and high-temperature stability, we propose hexaborides as promising candidates for photothermal applications due to their high oxidation resistance in air and good optical performance. Cerium hexaboride (CeB_6) is a rare-earth hexaboride with unique properties, such as high melting point and electric conductivity, offering a viable alternative to noble metals and refractory plasmonic materials for photonic and plasmonic applications. This material can be grown epitaxially under specific conditions, yielding high crystallinity and strong plasmonic polarizability within the infrared spectral region, which results in significantly improved optical properties.

Epitaxial CeB_6 thin films were fabricated using electron beam deposition, resulting in films with improved crystallinity and reduced optical losses. The design of thermal emitter microstructures is optimized based on electromagnetic simulations of our material. The fabricated devices exhibit a narrow peak with a tunable emission wavelength by modifying the structure parameters. This study demonstrates the potential of CeB_6 for high-temperature plasmonic applications. The results will advance the development of spectroscopic infrared thermal emitters, crucial for a wide range of industrial applications.

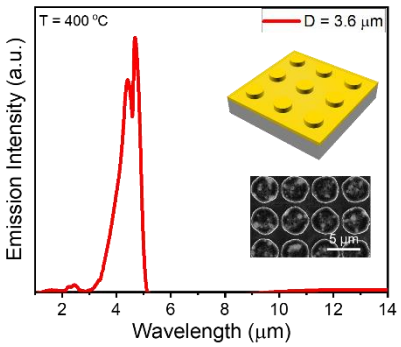

Figure 1: Schematics of a 2D-disc array thermal emitter device. SEM top image of a CeB_6-based thermal emitter. Emission spectra of wavelength selective emitters with different disk diameters.

References:

[1] T.D. Ngo, et al, Adv. Optical Mater., 10, 2201320 (2022)

[2] A. Ruiz-Perona, et al. Improving the optical response of epitaxial Cerium Hexaboride films for high-temperature plasmonic applications. ACS Applied Electronic Materials (Submited)

© 2025年 応用物理学会